Biochemical Pharmacology 81 (2011) 669–679

Contents lists available at ScienceDirect

Biochemical Pharmacology

journal homepage: www.elsevier.com/locate/biochempharm

Evaluation of *in vitro* PXR-based assays and *in silico* modeling approaches for understanding the binding of a structurally diverse set of drugs to PXR

Li Xiao, Elliott Nickbarg, Wenyan Wang, Ann Thomas, Michael Ziebell, Winfred W. Prosise, Charles A. Lesburg, S. Shane Taremi, Valerie L. Gerlach, Hung V. Le, K.-C. Cheng *

Merck Research Laboratories, K-15-2-2700, 2015 Galloping Hill Road, Kenilworth, NJ 07033, United States

ARTICLE INFO

Article history:
Received 14 October 2010
Accepted 2 December 2010
Available online 9 December 2010

Keywords:
CYP3A induction
Pregnane X receptor
In vitro assays

ABSTRACT

The pregnane X-receptor (PXR) is a promiscuous nuclear receptor primarily responsible for the induction of genes from the cytochrome P450 3A family. In this study, we used a previously described PXR/SRC tethered protein to establish two *in vitro* assays for identifying PXR ligands: automated ligand identification system (ALIS) and temperature-dependent circular dichroism (TdCD). *Kd* values determined by ALIS and TdCD showed good correlations with the EC50 values determined by a PXR luciferase reporter-gene assay for 37 marketed drugs. The same set of compounds was modeled into the PXR ligand-binding domain that takes into consideration the structural variations of five published X-ray structures of PXR–ligand complexes. Major findings from our *in silico* analysis are as follows. First, the primary determinants for non-binders of PXR are molecular size and shape of the compounds. Low molecular weight (MW $<$ 300) compounds were in general found to be non-binders, and those molecules that do not match the shape of the PXR ligand-binding site may also act as a non-binder. Secondly, the favorable hydrophobic interactions, mostly through aromatic π–π interactions, and the presence of suitable hydrogen bond(s) between the compounds and PXR are attributes of strong binders. Thirdly, the structures of the PXR binding domain possess the flexibility that accommodates structurally diverse compounds, while some of the strong binders may also adapt flexible conformations for fitting into the binding site. The results from this study provide a molecular basis for future efforts in reducing/abolishing the PXR-dependent CYP3A4 induction liability.

1. Introduction

Hepatic microsomal cytochrome P450 (CYP)3A is one of the major microsomal enzymes that is responsible for the metabolism of endogenous substrates and xenobiotics. In humans, CYP3A4 accounts for nearly half of the total abundance of microsomal CYP in the liver [1]. More importantly, CYP3A4 appears to be solely responsible for metabolism of 50% of the prescription drugs on the market. Hepatic expression of the CYP3A family in humans and in animals can be strongly induced by a wide range of structurally diverse compounds, many of which are also CYP3A substrates [2]. This induction represents a common type of drug–drug interaction with implications ranging from auto-induction to accelerating metabolism of a co-administered drug.

Induction of CYP3A is primarily controlled by a ligand-activated signal transduction pathway involving a nuclear receptor called the pregnane X receptor (PXR) [3]. Upon binding to a ligand, the PXR forms a heterodimer with retinoic X receptor (RXR). Further translocation of this heterodimer to the nucleus and binding to the xenobiotic responsive element located in the 5′-region of the CYP3A gene may lead to up-regulation of the transcription of the CYP3A gene [4]. Although induction of the CYP3A gene may be mediated by the interaction between the xenobiotic responsive element of the CYP3A gene and other receptors, such as constitutive androstane receptor (CAR) and vitamin D receptor (VDR) due to cross-talk, it has become clear that PXR plays a major role in the regulation of CYP3A [5].

During the binding of ligands, PXR also recruits steroid receptor coactivator (SRC) [6]. SRC-1 belongs to a family of coactivators that is characterized by multiple LXXLL motifs that bind to the AF-2 helix on PXR. This LXXLL motif interacts with two charged residues that are conserved among nuclear receptors on the surface of PXR forming a "charge clamp" that serves as a stabilizing force between

Abbreviations: PXR, pregnane X receptor; CYP, cytochrome P450; XRE, xenobiotic response element; SRC, steroid receptor co-activator; ALIS, automated ligand identification system; TdCD, temperature-dependent circular dichroism; *Kd*, dissociation constant; RXR, retinoic X receptor; CAR, constitutive androstane receptor; VDR, vitamin D receptor; LBD, ligand-binding domain; MW, molecular weight; Da, Dalton; DDI, drug–drug interaction.

* Corresponding author. Tel.: +1 914 552 8694; fax: +1 914 273 2724.
E-mail address: kccheng101@gmail.com (K.-C. Cheng).

0006-2952/$ – see front matter © 2010 Elsevier Inc. All rights reserved.
doi:10.1016/j.bcp.2010.12.003

PXR and SRC [7,8]. In the presence of a 25 amino acid fragment of human SRC-1, a PXR ligand, SR12813, is bound to the PXR–SRC-1 complex in a single orientation. This orientation is distinct from the multiple binding orientation of SR12813 in the absence of SRC-1. Thus, the presence of SRC-1 appears to limit the receptor's ability to breathe and helps to trap an active orientation of SR12813. In light of this finding, we previously designed a construct to express a tethered PXR–SRC protein and demonstrated its structural similarity to the normal PXR–SRC complex [9].

Several *in vitro* assays have been developed to understand the molecular mechanism of the induction of CYP3A4 [10–12]. These *in vitro* assays include a ligand-binding assay, a reporter-gene assay, a hepatocyte induction system, and a liver slice induction system. In this study, we utilized the previously described tethered PXR–SRC construct for two novel binding assays: ALIS and TdCD. Data presented here demonstrate a high degree of correlation between these binding data and the EC50 values obtained from a luciferase reporter-gene assay derived from a full-length native PXR, suggesting that the tethered PXR–SRC may resemble the putative PXR–SRC complex in ligand binding.

Several published X-ray structures [13–15,7] of the ligand-binding domain (LBD) of the human PXR protein revealed that PXR has a rather large and flexible hydrophobic ligand-binding site, the unique feature that makes it possible for PXR to harbor a variety of structurally diverse compounds, such as rifampicin. In previous studies, various ligand based *in silico* models, such as pharmacophore models [16], quantitative structure–activity relationship [17], and *in silico* machine learning approaches [18], were used to characterize the ligand–PXR interaction. Many of the studies were based solely on the compiled PXR activation data published elsewhere for modeling the ligand–PXR interaction. Due to variations in the methods used for determination of PXR activation, the only classification that could be made by these modeling exercises was that of activator versus non-activator. The absence of reliable quantitative comparison of the biological activity of ligands dampens the approach for building a quantitative *in silico* model for prediction of ligand–PXR interaction.

Using the data obtained from the experimentally measured assay from this study in a systematic fashion provided an important step forward to better understand PXR binding. We further attempted to correlate the physicochemical properties and the docking models of this set of the diverse marketed drugs with their complementing *in vitro* binding and functional data. In addition, structural variations of PXR in complex with different ligands were also taken into consideration. Through a combination of multiple computational approaches, we were able to differentiate these ligands into three categories, consistent with the experimental data, in particularly the non-binders and the strong binders. The molecular weights and shapes of the ligands, and favorable hydrophobic interactions are the primary determinants for PXR binding. In particular, aromatic interaction and hydrogen-bonds between the ligands and PXR were found to be important for strong binding. This study provides a basis to identify the molecular features for reducing the strong interactions between the PXR and the compounds in order to avoid the drug–drug interactions due to CYP3A induction caused by the activation of PXR.

2. Materials and methods

2.1. Chemicals

Pioglitazone and rosiglitazone were obtained from Biomol International LP (Polymouth Meeting, PA). Ritonavir was purchased from Sequoia Research Products (Berkshire, UK). Rifabutin was obtained from Apin Chemicals (Oxon, UK). Carbamazepine, dexamethazone, felodipine, haloperidol, and rifampicin were purchased from ICN Pharmaceuticals (Costa Mesa, CA). Other chemicals and reagents used in this study were obtained from Sigma Chemical Co. (St. Louis, MO).

2.2. Modeling of the 3-dimensional structures of PXR

The protein structure alignment tool in Maestro (Schrodinger LLC) was used to align the X-ray structures of PXR–SRC/SR12813 (PDB ID: 1NRL) and the tethered PXR–SRCp/SR12813 [9].

2.3. Affinity Selection-Mass Spectrometry (ALIS) system

In the ALIS process, a soluble target protein (1–10 μM) and a small molecule ligand or ligand mixture (0.05–50 μM) are first equilibrated in a suitable buffer [19,20], leading to the formation of a protein–ligand complex. The protein–ligand complexes are resolved from unbound compounds by rapid (<20 s) SEC using an Agilent 1100 HPLC system (Palo Alto, CA) equipped with a G1310A isocratic pump and G1322A solvent degasser and running at 0.3 mL/min. SEC columns were prepared in-house using proprietary techniques, but similar columns are available from Regis Technologies (Morton Grove, IL). Relatively weak non-specific compounds binding with high dissociation rates are lost during this fast separation process. The protein–ligand complex elutes in the void volume of the SEC column and is identified by UV absorption using a G1314A UV detector at 230 nm. The complex is captured in a collection loop, and transferred to a reversed-phase chromatography column (Targa-C18, 0.5 mm i.d. × 50 mm length, Higgins Analytical Inc., Mountain View, CA) and eluted using a gradient of 0–95% acetonitrile in water with 0.1% formic acid over 5 min with an Agilent G1376A binary pump running at 20 μL/min. Bound ligands are dissociated from the protein–ligand complex in the LC–MS via a combination of high temperature (60 °C) and acidic pH. A Waters LCT mass spectrometer (Manchester, UK), using a standard electrospray source running in positive ionization mode (capillary voltage = 3.5 kV and a source temperature of 180 °C, and 30 V cone and 3 V extraction lens settings), is used to scan from m/z 200 to 800 to identify and quantitate each released ligand using the compound-specific m/z value.

PXR protein–ligand binding reactions were prepared by equilibrating a diluted sample of PXR protein with a sample of ligand or ligands solubilized in aqueous buffer. 1 μL stock solutions (40 μM) of the appropriate compound in DMSO were diluted with 19 μL of 50 mM pH 8.0 Tris buffer containing 150 mM NaCl, 5 mM DTT, and 5% glycerol, and then clarified by centrifugation at 16,000 × g for 10 min. An aliquot of the resulting supernatant is then mixed with an equal volume of 5 μM PXR protein in the same buffer and incubated for 30 min at room temperature to ensure equilibration of the target protein with the small molecule compound. The samples are then chilled to 4 °C in preparation for AS-MS analysis using the system described above. Negative control experiments were performed for each compound by using a protein (invertase) that lacks affinity for the compounds of interest, but elutes at the same retention time on the SEC system as the target protein. In this fashion, it is possible to ensure that the expected MS signal is not derived from inadequate resolution of unbound compound (chromatographic breakthrough) of the ligand.

For *Kd* determinations, serial dilutions of a 1 mM compound stock in DMSO were prepared, diluted 20-fold with Tris buffer, and mixed 1:1 with 5 μM PXR and then equilibrated and analyzed as described above. By increasing the concentration of compound relative to a constant concentration of target protein and saturating the protein receptor, and then measuring the amount of ligand released from the protein–ligand complex using AS-MS, we can generate a hyperbolic binding curve for each compound

and derive the apparent *Kd* from the shape of the curve, as described previously [21,22].

2.4. Temperature dependent circular dichroism (TdCD)

Circular dichroism spectra were recorded in the 200–300 nm wavelength range in a buffer containing 25 mM HEPES, pH 7.9, 5% (v/v) glycerol, 150 mM NaCl, and 5 mM DTT, in a Jasco J-810 spectrapolarimeter. The thermal scan was performed in a 1 mm cuvette, containing 2.5 μM of PXR–SRC tethered protein, and 25 μM of the tested compound. The solution containing the compound and the protein was incubated at room temperature for 10 min before the thermal denaturation was carried out. The ellipticity at 220 nm was scanned using a response time of 4 s. Continuous monitoring of the thermal transition at a constant rate of 2 °C/min was performed by a PTC-424S automatic Peltier. The data were analyzed using the JASCO software assuming a two-state reversible equilibrium transition [23].

2.5. Reporter gene assay

DPX2 cells (Puracyp Inc.) were seeded in 96-well plates with 2.5×10^4 cells/well 24 h prior to adding compounds at various concentrations [10]. The cells were incubated at 37 °C for 48 h. Afterwards, the cells were washed with phosphate buffered saline (PBS). The luciferase activity was detected by adding the Bright-glo solution (Promega) prior to scanning by a luminomitor. The fold of induction was calculated based on the ratio between the luminescence from cells treated with compounds and the luminescence from cells treated with DMSO. The rifampicin ratio was calculated based on fold of induction of test compound/maximum fold of induction for rifampicin.

2.6. 2D structures, physical chemical properties and clustering

The 2D structures of the ligands were retrieved from Mddr3d public (MDL) ISIS database. Pipeline pilot (Accelrys) protocols were used to calculate the physicochemical properties of each ligand from its 2D structure, including molecular weight (MW), clogP, numbers of hydrogen bond (Hbond) donors, Hbond acceptors and rotatable bonds, molecular surface area, and polar surface area. To categorize the ligands into different clusters, the tanimoto similarity comparison of the ligands was carried out using pipeline pilot ECFC_4 fingerprint.

2.7. 3D structure generation of market drugs

Both LigPrep (Schrodinger) and Concord program (Concord Software, CA) were used to generate the 3D structures of the ligands from their 2D structures. In LigPrep, the MMFFs forcefield and the Epik program for ionization state of the ligands were applied. Different tautomers of the ligands were also included in the 3D structure generation.

2.8. Docking calculations

The following six PXR X-ray crystal structures (Fig. 7) in the PDB are available for template selection of the docking studies: hyperforin (1M13.pdb), colupulone (2QNV.pdb), rifampicin (1SKX.pdb), SR12813 (1NRL.pdb), and T0901317 (2o9i.pdb). Differences in these structures induced by different bound ligands were observed. For example, as shown in Fig. 7a, among the six different structures, they displayed a 5.7 Å shift in the His407 side-chains, a 7 Å shift in the Met323 aliphatic long side-chains, and 2 Å shifts in several Phe side-chains.

To accommodate the structural variations, we included all six X-ray structures in our docking calculations for all 37 of the marketed drugs. For selecting the final docking poses for the ligands with the best docking scores, we also took into account the chemical structure similarity between the bound ligand in that particular X-ray structure and our ligands using tanimoto similarity coefficients with Pipeline pilot (Accelrys). The chemical

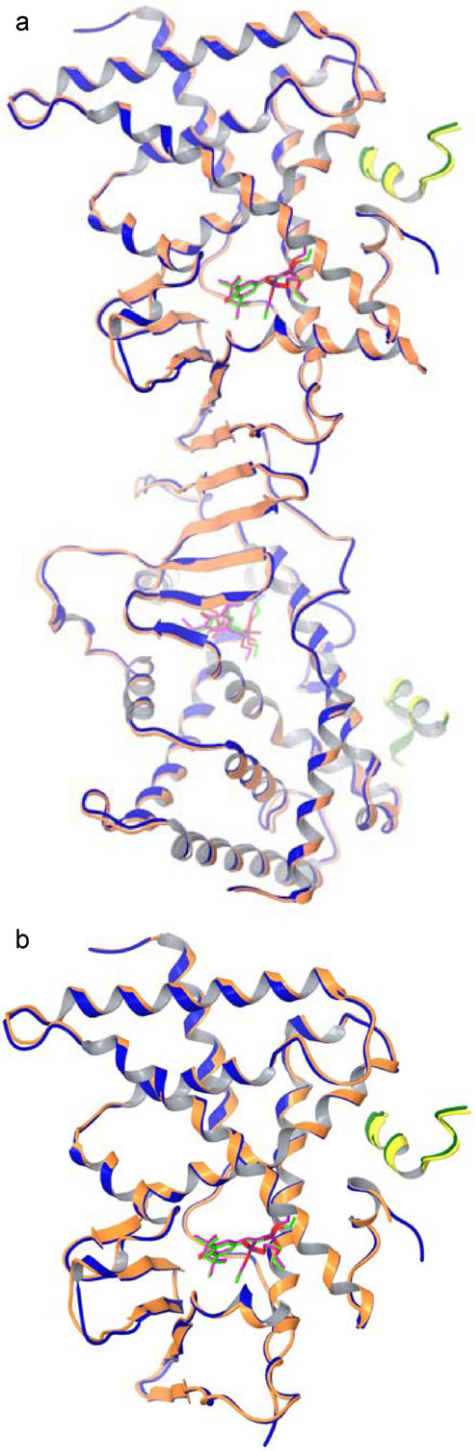

Fig. 1. Overlay of the X-ray structures of PXR–SRC/SR12813 (PXR, blue; ligand, green; SRC peptide; dark green) and tethered PXR–SRC peptide/SR12813 (PXR, orange; ligand, magenta; SRC peptide, yellow). (a) The homodimer structures. (b) The monomer structures. (For interpretation of the references to color in this figure legend, the reader is referred to the web version of the article.)

structures of the bound ligands in the five X-ray structures of PXR are included in Fig. 1b. The computer docking program Glide (Schrodinger LLC) was used and rigid docking with the XP mode was selected for docking the ligands. The centroid of the bound ligand in the X-ray structure defined the binding site as a 12 Å × 12 Å × 12 Å cubic box. Ten poses of each ligand were evaluated from each docking run.

3. Results

3.1. Structural identity between the native PXR–SRC complex and the PXR/SRC tethered protein

As previously reported, we have expressed a PXR/SRC tethered protein and determined the 3-dimensional crystal structure [9]. A more detailed comparison among the native PXR complex with S12813, PXR–SRC with SR12813 and the PXR/SRC tethered with SR12813 is shown in Fig. 1. The crystal structures of the later two proteins appear to be very similar with a rmsd of 0.29 Å over 259 matching Cα atoms. In addition, the orientation of SR12813 in the binding sites of these two proteins appears to be identical. However, comparison between the native PXR without the SRC and the PXR/SRC tethered protein showed significant differences in the backbone structure, the shape and the volume of the corresponding ligand binding sites (data not

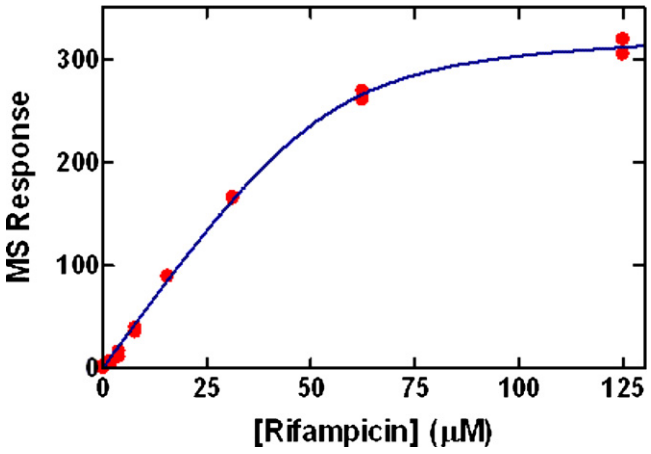

Fig. 2. ALIS binding of rifampicin to the tethered-PXR–SRC at 25 °C.

Table 1
Summary of the *Kd* and EC50 values of 37 marketed compounds in ALIS, TdCD, and reporter-gene assays, and their molecular weight (MW) and molecular surface area (MolSurf). Strong PXR binders are indicated in red color, moderate binders in blue color, and non-binders in black.

Compounds	*Kd* TdCD (μM)	*Kd* ALIS (μM)	EC50 (μM)-reporter-gene assay	MW (Da)	MolSurf
Amoldipine	0.58	23.5	1.6	408	408
Caffeine	3.3	>200	>200	194	201
Clotrimazole	0.29	0.33	1.3	344	321
Dexamethazone	9.5	>200	>200	392	372
Diclofenac	1.7	>200	>200	295	270
Doxorubicin	16	>200	>200	543	504
Felodipine	0.13	0.81	0.25	384	367
Haloperidol	0.75	3.35	4.2	375	354
Hyperforin	0.05	N/A	0.2	536	600
Isradipine	0.15	2.03	0.67	371	365
Lacidipine	0.05	0.03	0.32	455	477
Lansoprazole	4.9	40	6.5	369	325
Mifepristone	0.43	2.88	3.1	429	427
Naproxen	2.1	>200	>200	216	223
Nicardipine	0.11	0.42	0.4	479	481
Nifedipine	1.2	1.3	2.2	346	346
Nimodipine	0.09	0.276	0.45	418	424
Nisoldipine	0.25	1.6	1.9	388	394
Nitredipine	0.25	1.66	3.0	360	360
Omeprazole	5.7	1.66	21	345	340
Phenylbutazone	4.5	53	36	308	295
Phenytoin	7.8	>200	45	252	230
Pioglitazone	4.8	29.78	>200	356	337
Pregnenalone	0.87	>200	100	316	317
Probenecid	11	>200	>200	285	281
Rifabutin	0.19	4.3	0.2	847	838
Rifampicin	0.54	10	0.7	822	820
Ritonavir	0.1	0.57	0.8	720	717
Rosiglitazone	0.92	2.2	49	357	337
Sulfamethazine	8.6	>200	190	278	265
Sulfasalazine	2.6	>200	>200	398	356
Sulfinpyrazone	1.8	9.4	28	404	364
Terbinafine	0.6	0.25	16	291	323
Theophylline	3	>200	>200	180	180
Tolbutamide	2.3	>200	>200	270	264
Troleandomycin	0.43	13.79	4.5	813	825
Verapamil	0.53	10.2	9.5	454	497

shown). The effect of SRC on PXR is demonstrated by the shapes of the PXR ligand binding domain. In the absence of SRC the ligand binding site is less restricted than in the presence of SRC, suggesting that SRC may play a role in more restricted and specific ligand binding.

3.2. Automated ligand identification system (ALIS)

Specific ligand binding to a given receptor may be evaluated using the ALIS to separate the free and the bound ligands. Simultaneously, the ligand is identified using a mass spectrometer. Based on mass spectrometry quantification, a *Kd* value may be estimated according to the ligand binding curve shown in Fig. 2. The *Kd* value determined using ALIS methods represents a direct measurement of the binding affinity. In contrast, other competitive binding assays may represent an indirect measurement of the binding affinity of a ligand for PXR.

The *Kd* determined by the ALIS method is shown in Table 1. The most potent compound based on the ALIS method is lacidipine with a *Kd* of 0.03 μM. Compounds that showed no detectable biding to PXR over a concentration range of 0.01–200 μM in the ALIS were designated as negatives.

3.3. Temperature-dependent circular dichroism (TdCD)

The interaction between ligands and purified PXR/SRC tethered protein was evaluated by circular dichroism. As shown in Fig. 3, a single unfolding transition phase was observed for the tethered protein in the absence of any ligand with a melting temperature (T_m) of 41.5 °C. The T_m increased to 49 °C in the presence of 25 M of rifampicin, indicating that rifampicin binding to the tethered PXR/SRC may improve the thermal stability of the complex. In the presence of ritonavir and hyperforin, a slightly better thermal stability was observed in comparison with rifampicin (Fig. 3). Hypothetical *Kd* values were calculated based on the shift of the T_m in presence of various compounds (Table 1). The range of the hypothetical *Kd* values for the 37 marketed compounds examined appears to be narrower than those for the *Kd* values determined by ALIS, and hence, it may be treated as a ranking order instead of an estimation of the binding affinity.

3.4. PXR reporter-gene activity

A stable full-length native PXR construct expressed in HepG2 cells was used to determine the reporter-gene activity of various ligands. The activity of luciferase is expressed as a "rifampicin ratio", which is normalized after comparing with the maximal rifampicin-induced luciferase activity in each batch to reduce the batch-to-batch variation. Fig. 4 shows the concentration versus response curves of four compounds. Three of the compounds, rifampicin, hyperforin, and ritonavir, display typical luciferase activating activity (rifampicin ratio elevation), which allows for the determination of EC50 values. Theophylline did not elicit any reporter-gene activity above the solvent control, and, therefore, is considered to be unable to interact with PXR. It should be pointed out that neither ritonavir nor hyperforin reached the same maximal luciferase as rifampicin, suggesting that these compounds may act as partial agonists in the reporter-gene assay. The EC50 values of the 37 compounds examined are shown in Table 1. Based on the EC50 values, the compounds were divided into three categories: strong (EC50 ≤ 1 μM) in red color, moderate and weak in blue color (1 μM < EC50 ≤ 100 μM), and negative in black color (EC50 > 100 μM). The strong ligands identified by the reporter-gene-assay are: felodipine, hyperforin, isradipine, lacidipine, nicardipine, nimodipine, rifabutin, rifampicin, and ritonavir; the

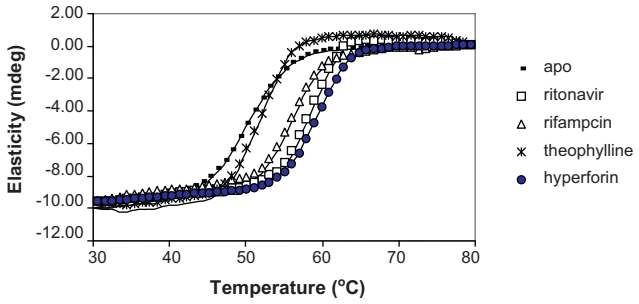

Fig. 3. Temperature-dependent circular dichroism of rifampicin, ritonavir, hyperforin, and theophylline following incubation with the tethered-PXR–SRC apoprotein.

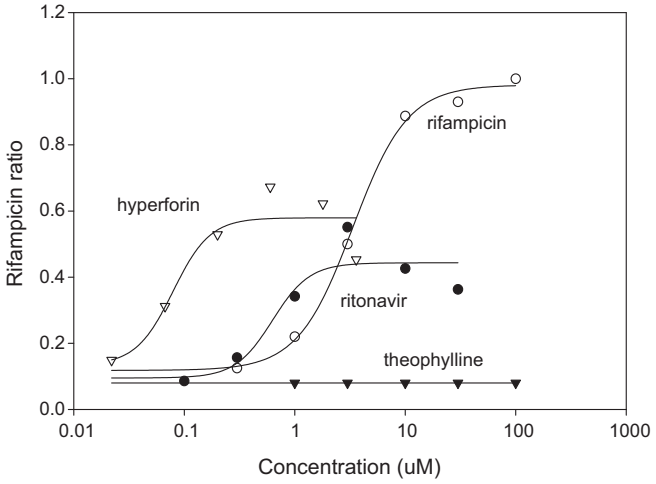

Fig. 4. PXR-dependent reporter-gene activity of rifampicin, ritonavir, hyperforin, and theophylline. The reporter gene response was normalized against the maximal response of rifampicin. The rifampicin ratio was plotted against the concentrations of the compound used in treatment of the HepG2 cells.

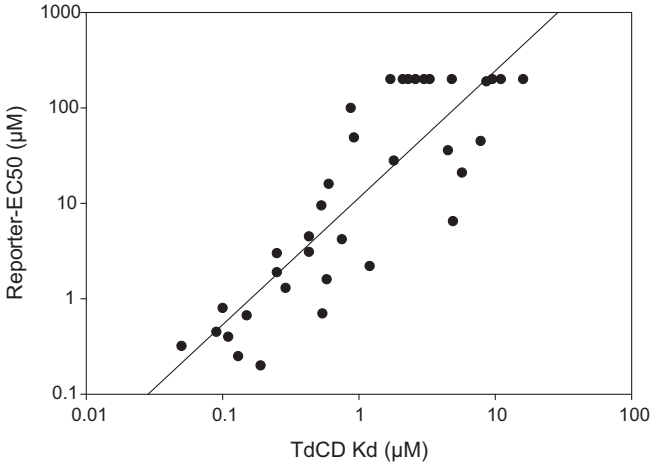

Fig. 5. Regression analysis of the correlation between the *Kd* values obtained using TdCD and the EC50 values obtained using the PXR reporter-gene assay to characterize 37 marketed compounds ($r^2 = 0.73$). Compounds with EC50 values >200 μM using the reporter-gene assay are assigned an EC50 = 200 μM in this plot.

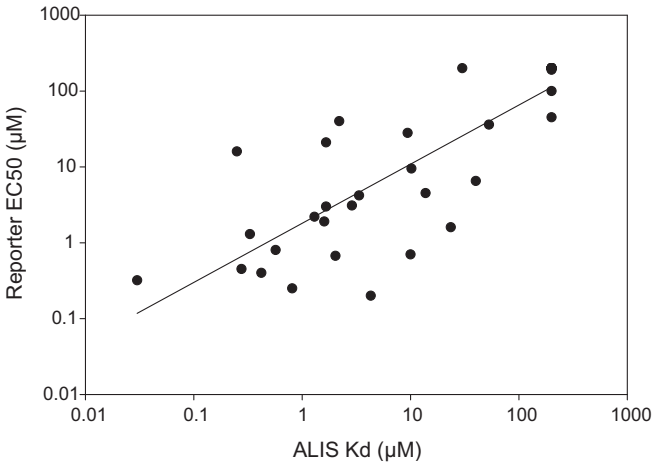

Fig. 6. Regression analysis of the correlation between the *Kd* values obtained using ALIS and the EC50 values obtained using the reporter-gene assay to examine 37 marketed compounds ($r^2 = 0.68$). Compounds with EC50 values >200 μM using the reporter-gene assay or with *Kd* values >200 μM using the ALIS are assigned an EC50 = 200 μM in this plot.

moderate/weak ligands are amoldipine, clotrimazole, haloperidol, lansoprazole, mifepristone, nifedipine, nisoldipine, nitredipine, omeprazole, phenylbutazone, phenytoin, rosiglitazone, sulfinpyrazole, terbinafine, troleandomycin, and verapamil; and the negatives are: caffeine, dexamethazone, diclofenac, doxorubicin, naproxen, pioglitazone, probenecid, sulfamethazine, sulfasalazine, theophylline, and tolbutamide.

3.5. Comparison of multiple PXR assays

The correlation between these *in vitro* assays was evaluated using linear regression analysis of the binding affinity (*Kd*) values and the potency (EC50) values. As shown in Fig. 5, a good correlation ($r^2 = 0.72$) was observed between the estimated *Kd* based on TdCD and the EC50 determined by the PXR reporter gene assay of 37 marketed compounds. This suggests that the PXR–SRC tethered protein parallels the binding property of the native PXR in the PXR reporter gene assay.

When the *Kd* value obtained using the ALIS assay was compared in a linear regression analysis with the EC50 in the PXR reporter gene assay, a moderate correlation with a r^2 value of 0.67 was observed with 37 marketed compounds (Fig. 6). This finding further suggests that the PXR–SRC tethered protein resembles the native PXR in functionality of ligand binding.

3.6. Classification of strong, moderate/weak and non-binders

Using the EC50 cut-off presented in Table 1 as a guide, the cut-offs for the hypothetical *Kd* values obtained using TdCD are suggested as follows: strong ($Kd < 0.2$ μM), moderate/weak (0.2 μM $\leq Kd \leq 2$ μM), and negative ($Kd > 2$ μM). The cut-offs for the *Kd* values obtained by ALIS appear to be similar to that of luciferase reporter gene assay: strong ($Kd < 1$ μM), moderate/weak (1 μM $\leq Kd \leq 100$ μM), and negative ($Kd > 100$ μM). Based on the overall binding affinities and PXR-reporter activities, we categorize these 37 ligands (Fig. 8) in three categories: strong, moderate, and non-binder. For strong binders, the cut-off ($Kd < 1$ μM and/or EC50 < 1 μM) was required to have been achieved in two out of the three parameters tested (ALIS *Kd*, TdCD *Kd*, and reporter EC50). For moderate binders, the cut-offs were 1 μM $< Kd < 100$ μM and/or 1 μM $<$ EC50 < 100 μM. For non-binders, all of the *Kd* and EC50 values must have been >200 μM. According to these criteria, 10 compounds studied were found to be strong binders, 15 were moderate binders, and 12 were non-binders.

3.7. Correlation between binding affinity and physical/chemical properties

The physical/chemical properties (e.g., MW, clogP, number of Hbond donors, number of Hbond acceptors, number of rotatable bonds, and molecular surface area) of each of the 37 marketed drugs were determined as described in Section 2. Each of the physical/chemical properties was compared with the PXR ALIS or TdCD binding affinity data. Results from this analysis indicated that the only physical/chemical properties related to strength of PXR binding were the MW and the molecular surface area (Table 1). Other physical/chemical properties, such as ClogP, showed no correlation with PXR binding potency (data not shown).

3.7.1. Low molecular weight (MW) compounds lack PXR binding affinity

As shown in Table 1, among 12 non-binders eight compounds have MW < 300 Da. These include caffeine (MW, 194 Da), naproxen (MW, 216 Da), diclofenac (MW, 295 Da), probenecid (MW, 285 Da), sulfamethazine (MW, 278 Da), theophylline (MW, 180 Da), tolbutamide (MW, 270 Da), and phenytoin (MW, 252 Da). One exception is terbinafine, which is classified as a moderate binder (ALIS *Kd* = 0.25 μM and PXR reporter EC50 = 16 μM) but has a MW of 291 Da. The molecular surface area of each of these compounds correlates very well with low molecular weight, suggesting that they also have lower molecular surface areas (Table 1, Fig. 9).

The lack of binding affinity between each of these small molecules and PXR was further investigated to determine if insufficient physical interactions is the reason. When compounds are too small, they may occupy only part of the large PXR LBD as is illustrated by analysis of the interaction of caffeine within the PXR binding cavity in Fig. 10. The binding energy, due to van der Waals interactions, appears to below a meaningful interaction between caffeine and PXR. For example, the size difference between the PXR LBD and caffeine cavity may be too large to accommodate the binding of caffeine.

3.7.2. Mismatched molecular shape disrupts interaction with PXR

Several larger molecules with molecular weights greater than 300 (e.g., dexamethazone, doxorubicin, sulfazalazine and pioglitazone) are also shown to be incapable of interacting with PXR. These compounds are classified as non-binders due to high ALIS and TdCD *Kd* values, and low/no signal in the PXR reporter assay. Comparison of the molecular shapes of these compounds and the PXR LBD reveals some significant differences. Their molecular shapes (Fig. 11) of these compounds are linear and/or elongated in one dimension, resulting in mismatch with the PXR LBD.

3.8. Structural modeling of PXR strong binders

3.8.1. Hyperforin and rifampicin

In agreement with previously published data, both hyperforin and rifampicin are strong PXR binders with measured EC50 values of 0.2 μM and 0.7 μM, respectively, in the PXR reporter assay. The molecular weight (536 Da) of hyperforin is much lower than that of rifampicin (822 Da), as is its molecular surface area. Rifampicin, due to its larger surface area, makes more contacts with the active site residues in PXR than hyperforin, while the same four hydrogen bonds observed in PXR/rifampicin complex are also observed in PXR/hyperforin structure. These four hydrogen bonds may provide better binding interactions for these two molecules.

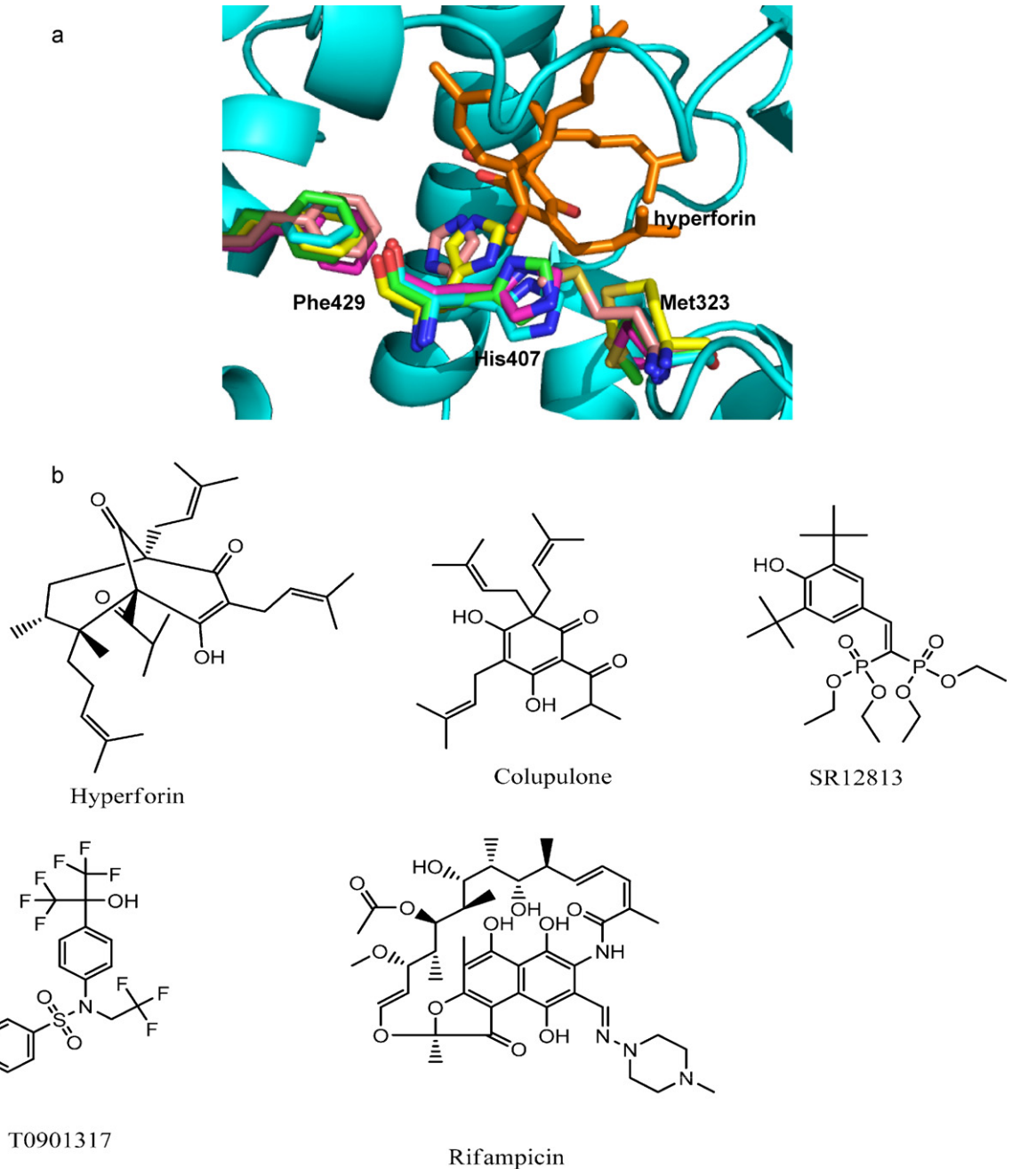

Fig. 7. Composite structure of five X-ray structures of PXR complex with ligands obtained from PDB (a). The backbone ribbon structures were aligned together with flexible side chain structures of Phe249, Met323 and His407. Hyperforin is shown in the center of the ligand binding cavity. The 2D chemical structures of the ligands complexes with PXR are shown in (b).

3.8.2. Rifabutin

Rifabutin is an analog of rifampicin, and its binding affinity for PXR is comparable to that of rifampicin (EC50 = 0.2 μM and ALIS *Kd* = 4.3 μM). The structural difference between rifabutin and rifampicin is at the substitution of the conjugate naphthalene ring (Figs. 7b and 8). Based on ligand docking results, rifabutin binds to PXR in a similar fashion as rifampicin with strong hydrophobic interactions through extended contacts between its macrolide ring and the residues in the PXR LBD (data not shown).

3.8.3. Ritonavir

Ritonavir binds strongly to PXR with an EC50 of 0.8 μM in the PXR report assay and ALIS *Kd* value of 0.57 μM. The molecular weight of ritonavir (717 Da) and its size are intermediate between those of rifampicin and hyperforin. Ritonavir is a peptidic compound posing two di-peptide bonding. Based on tanimoto similarity, only T0901317 (2o9i.pdb) was found to display similar structural features as ritonavir. Therefore, we selected the binding model (Fig. 12) of ritonavir based on the docking poses in the T0901317/PXR structure. The binding model reveals several distinct features of the ritonavir/PXR complex, which includes two hydrogen bonds between ritonavir and residues Gln285 and His327. In order to provide best fit into PXR, ritonavir will have to fold into a U-shaped structure. The un-substituted thiazole end of ritonavir appears to insert itself into the site lined with Phe429, Phe251, His407, Phe281, His327, Trp299, and Tyr306, forming favorable aromatic interactions, whereas the isopropyl-substitut-

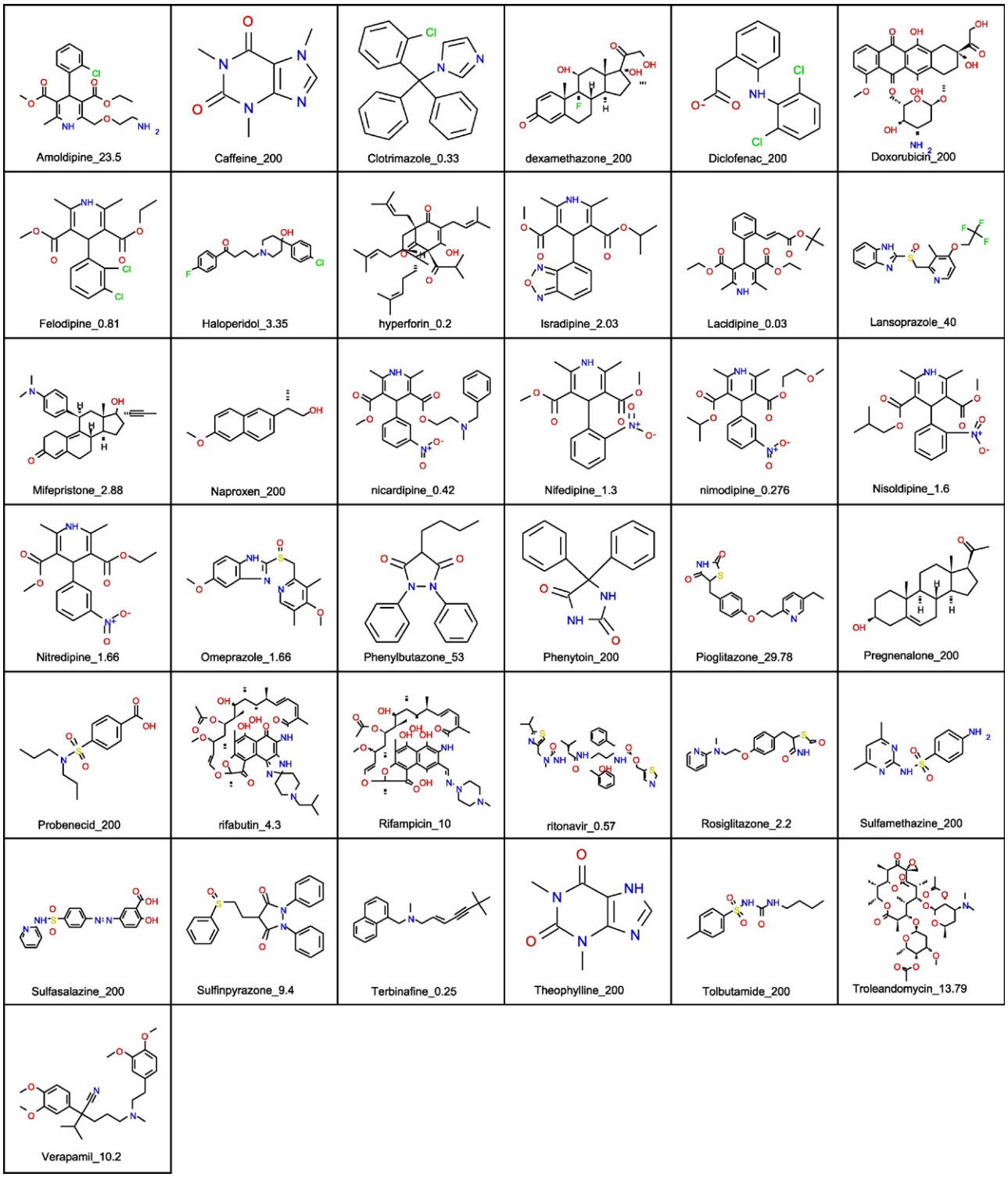

Fig. 8. 2D chemical structures of 37 drugs evaluated in this study. The EC50 based on the PXR reporter gene activity is shown after the name of individual drug.

ed thiazole end is making contact with Lys210 and Leu240. This model indicates that the strong interaction between ritonavir and PXR is predominantly due to a combination of hydrophobic interactions and multiple hydrogen bonds.

3.8.4. Clotrimazole

The results from the ALIS assay (Kd = 0.33 μM) confirmed that clotrimazole is a PXR strong binder. Based on the tanimoto similarity, T0901317 (2o9i.pdb) was defined as the sole ligand comparable to clotrimazole. Therefore, we selected the binding model of clotrimazole from the docking poses collected from the PXR/T0901317 structure. As shown in Fig. 13, the imidazole moiety of clotrimazole forms a hydrogen bond with Gln285. Five aromatic residues in PXR (Phe281, Phe288, His407, Tyr306, and Trp299) interact with four aromatic rings in clotrimazole through π–π stacking interactions. In addition, Met323 and Leu209 contribute favorable van der Waals hydrophobic interactions between clotrimazole and PXR.

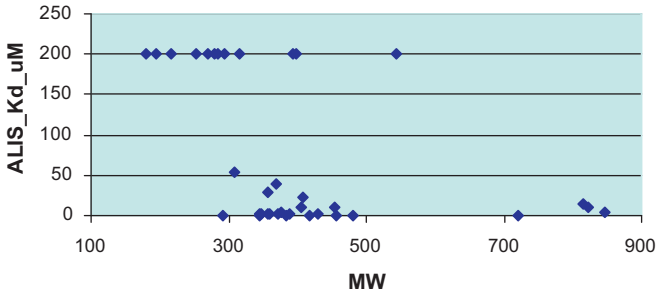

Fig. 9. Relationship between molecular weights and binding affinity of ligands to PXR based on ALIS.

3.8.5. Ca^{++} channel blockers

Among ten strong PXR binders, five belong to the Ca^{++} channel blockers, namely – felodipine, isradipine, lacidipine, nicardipine, and nifedipine. The molecular weights of these drugs range from 350 to 481 Da. Felodipine, isradipine, lacidipine, nicardipine, and nifedipine show tanimoto similarity with SR12813 (1NRL.pdb), colupulone (2QNV.pdb), and rifampicin (1SKX.pdb). Following inspection of the binding models in each of the three X-ray structures for these five ligands, those modeled in PXR/SR12813 structure appeared to correlate best. Hence, we present detailed interactions of these five ligands modeled binding to PXR based on the PXR/SR12813 complex structure. The common feature that was observed in the docking models of all five ligands is that the N atom in the pyridine core (2,6-dimethyl-1,4-dihydropyridine) of all five compounds forms a hydrogen bond with Ser247 side-chain of PXR. This hydrogen bond appears to act as a primary anchor for positioning the ligand in PXR LBD.

3.8.5.1. Felodipine. Felodipine is a PXR strong binder with an EC50 value of 0.25 μM in the PXR reporter assay. Similar to SR12813, felodipine interacts with PXR through mostly hydrophobic interactions. As shown in Fig. 14, the binding of felodipine involves residues Leu209, Met243, Met246, Ser247, Phe281, Gln285, Phe288, Trp299, Tyr306, His327, Leu324, Met323 His407of PXR, whereas the hydrogen bond with Ser247 in PXR serves as the anchor for ligand binding. In addition, one of felodipine's dimethyl groups makes hydrophobic interactions with Met243.

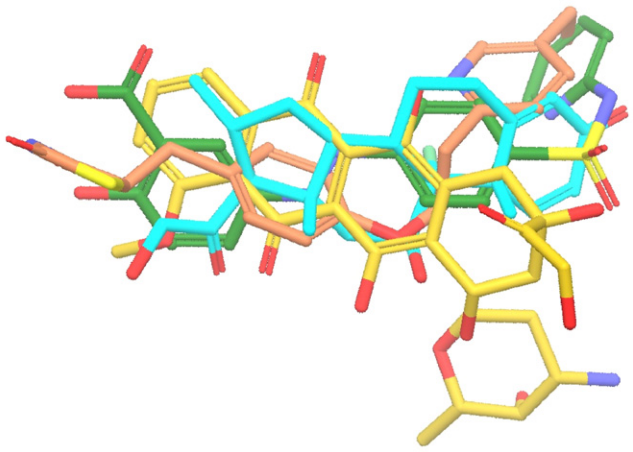

Fig. 11. Overlapping 3D structures of dexamethazone, pioglitazone, doxorubicin, and sulfazalazine. Stick structures of the structures are shown in blue (dexamethazone), brown (pioglitazone), yellow (doxorubicin), and green (sulfazalazine). (For interpretation of the references to color in this figure legend, the reader is referred to the web version of the article.)

3.8.5.2. Lacidipine. Both lacidipine and felodipine share the same dimethyl pyridine core. The only structural difference between the two ligands is on the substitution on the phenyl ring. Felodipine has an ortho and meta di-cloro-phenyl ring, while lacidipine an ortho t-butyl but-2-enoate substitution. The ortho t-butyl but-2-enoate fits into the binding pocket surrounded by Leu206, Leu209, Lys210, Val211, Ile236, Phe237, Ser238, Leu240 and Met243. As predicted by the binding model, lacidipine shows high affinity to PXR, with the lowest EC50 (0.32 μM) and *Kd* in ALIS (0.03 μM).

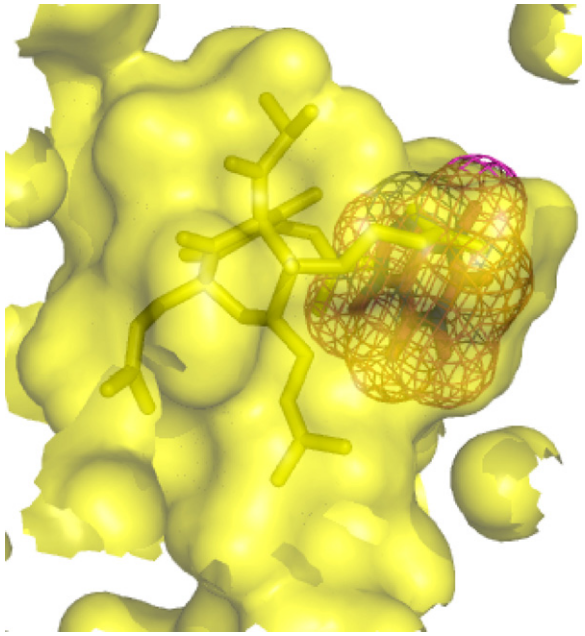

Fig. 10. Complex structures of PXR/hyperforin and a hypothetical docking of caffeine in the ligand binding cavity. The ligand binding cavity of PXR is shown in shade. Hyperforin is shown as a stick structure in the center of the ligand binding cavity. Caffeine as encircled by a nest is shown to occupy the right side of the ligand binding cavity.

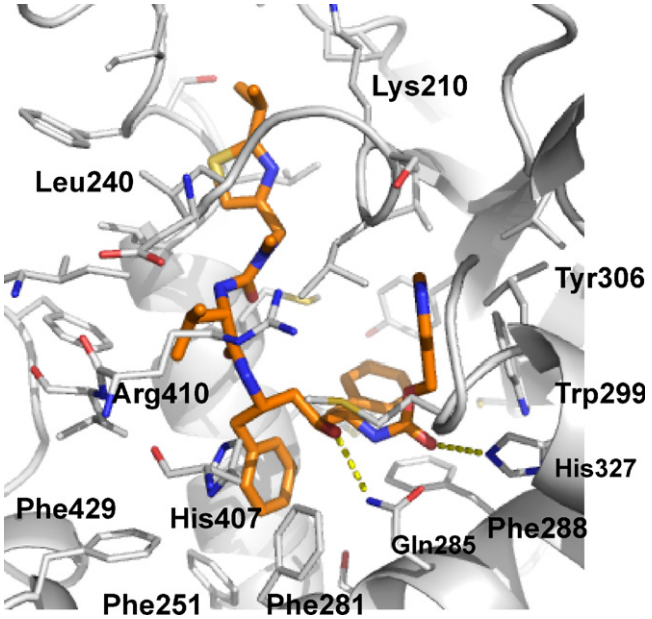

Fig. 12. Docking structure of ritonavir in the ligand binding cavity of PXR. Ritonavir in stick structure is shown in the center of the ligand binding cavity. Amino acid residues interacting with ritonavir in the ligand binding cavity are highlighted.

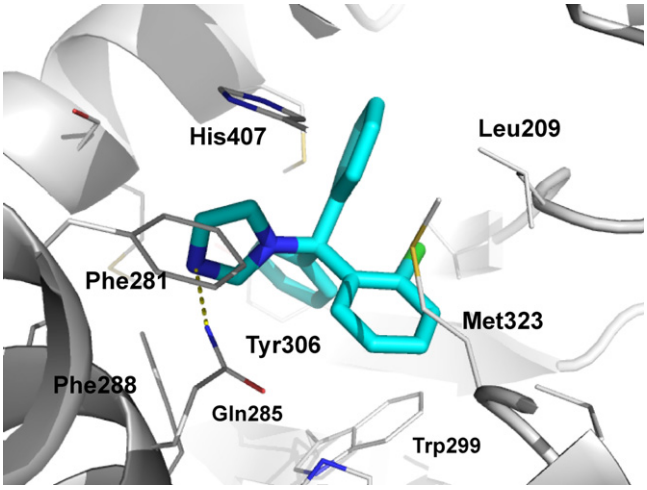

Fig. 13. Docking structure of clotrimazole in the ligand binding cavity of PXR. Clotrimazole in stick structure is shown in the center of the ligand binding cavity. Amino acid residues interacting with clotrimazole in the ligand binding cavity are highlighted.

3.8.5.3. Isradipine. Isradipine is another PXR strong binder, with low EC50 (0.67 μM) and *Kd* in ALIS (2.03 μM). The compound has a dimethyl pyridine core that is shared by felodipine and lacidipine, but has a unique bicyclic benzooxadiazole ring. The binding model shows that the benzooxadiazole ring overlaps with the di-cloro-pyridine of felodipine binding model of felodipine, and points toward Gln285 of PXR. The oxygen atom in the oxadiazole ring of isradipine may form a hydrogen bond anchor with the nitrogen atom on the Gln285 side chain.

3.8.5.4. Nimodipine. Nimodipine shows only a slightly different 3-substitution on the dimethyl pyridine ring from other analogs. The binding model is anticipated to be similar to those of the analog series. In the model, the meta-nitro substitution on the benzyl group is located next to Gln285, and may form a hydrogen bond anchor with the nitrogen atom in the Gln285 side chain.

3.8.5.5. Nicardipine. Nicardipine is the largest molecule of the series, with a 3-benzyl amino ethyl acetyl substitution on the pyridine group. The docking model revealed that this large side-chain may alter its binding mode to PXR. Instead of binding to Ser247 of PXR, the nitrogen atom in the pyridine core of nicardipine appears to move away from Ser247, and toward Gln285 of PXR. The oxygen atoms on the meta-nitro substitution on the benzyl group may form hydrogen bonds with the backbone nitrogen of Leu411 and the imidazole group of His407 in PXR. The large 3-group tugs inside the binding site forming π–π stacking between the benzyl group and the aromatic side-chains of Phe288, Tyr306, and Trp299 in PXR (data not shown).

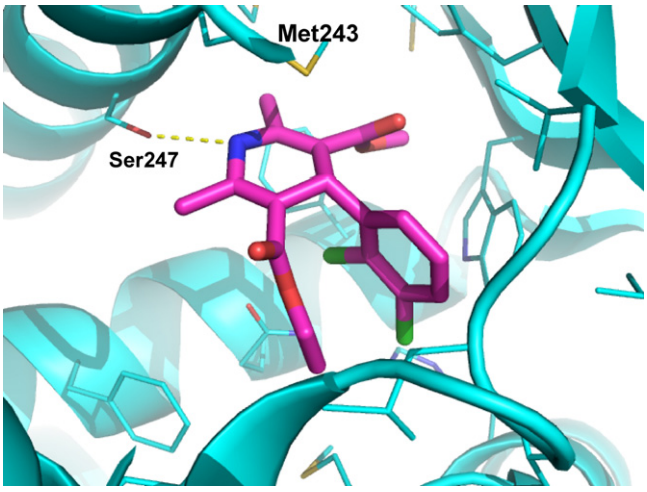

Fig. 14. Docking structure of felodipine in the ligand binding cavity of PXR. Felodipine in stick structure is shown in the center of the ligand binding cavity. Amino acid residues interacting with felodipine in the ligand binding cavity are highlighted.

Table 2
PXR docking score of calcium channel blockers.

Ligand	XP GSscore	Glide evdw	Glide evdw	ALIS *Kd* (μM)
Lacidipine	−7.666164	−54.758078	−2.540762	0.03
Nimodipine	−6.753223	−46.042701	−4.390401	0.27
Nicardipine	−6.224779	−51.060739	−3.060118	0.42
Felodipine	−6.210285	−39.570914	−1.565818	0.81
Isradipine	−6.065332	−40.148559	−2.156376	2.03
Nifedipine	−5.833937	−42.121803	−3.567011	1.3
Nisoldipine	−5.749992	−43.37405	−4.565354	1.6
Nitrendipine	−5.60046	−41.88387	−2.318551	1.7

3.9. Moderate binders to PXR

Four of the Ca^{++} channel blocker analogs – nifedipine, nisodipine, nitredipine, and amoldipine, are moderate binders. Three of these analogs – nifedipine, nisoldipine, and nitredipine, are very similar to nimodipine. Their binding modes are therefore expected to be similar to that of nimodipine. It appears that shift of the nitro-substitution from the meta- to the ortho-position on the phenyl ring may have little effect on binding to PXR. In the case of amoldipine, the binding mode may be different due to its long alkyl side chain which replaces one of the methyl groups on the pyridine of nimodipine. This bulky group may hinder the binding to PXR, and thus, reduces its binding affinity. The other eleven moderate binders are structurally diverse. Docking scores shown in Table 2 appear to correlate with the binding affinity as measured by ALIS. Examination of the binding models for these drugs revealed that the interactions with PXR are predominantly hydrophobic interactions, which include van der Waals contacts and π–π stacking. A more definitive evaluation of the binding models may require additional information on the structure–activity relationship.

4. Discussion

The pregnane X receptor (PXR) belongs to the nuclear receptor (NR) superfamily which comprises about more than 70 members. Closely related to PXR are CAR, VDR, ER, and PPAR [24,25]. These receptors contain two distinct structural domains: a DNA-binding domain and a ligand-binding domain. Upon binding to a ligand, the receptor forms a heterodimer with retinoic X receptor (RXR) prior to translocation into the nucleus. Once in the nucleus, the PXR–RXR complex binds to the xenobiotic responsive element (XRE), which results in the up-regulation of transcription of the CYP3A4 gene and a range of other genes. In addition its formation of heterodimer with RXR, PXR is also known to form complexes with the SRC. In the presence of SRC, the flexibility of the ligand-binding pocket of PXR appears to be more restricted based upon the crystal structure of the PXR–SRC complex. SRC contains a LXXLL motif that adopts an α-helical conformation and binds to the surface of PXR forming a "charge clamp" as observed in several other NR–SRC complexes [26,27]. As previously demonstrated, the 3-dimensional structure of the tethered PXR–SRC construct that we made was nearly identical to that of the reported PXR–SRC complex. Furthermore, the binding of SR12813 in a PXR–SRC complex is similar to that of the tethered PXR–SRC construct. The results from this study provide additional ligand-binding evaluation using the tethered

PXR–SRC construct. Comparison of the tethered construct-based *Kd* values and the EC50 values obtained using a reporter-gene assay with full-length native PXR demonstrated a good correlation, supporting the conclusion that the tethered PXR–SRC construct is an excellent model for the interaction between ligands and PXR.

The consequence of the ligand binding to PXR in the liver triggers the induction of a large array of genes that lead to adverse effects in the elevation of drug metabolism activity and potential drug–drug interactions. In drug discovery, enzyme induction caused by PXR activation represents a major obstacle. The most critical issue appears to be how to use the binding data to aid in the structural design because it is impossible to determine the 3-dimensional structures of every ligand–PXR complex. The *Kd* ranges for its ligands range from low nanomolar to high micromolar. This wide range of binding affinity, especially for highly structurally diverse compounds, may complicate the understanding of the molecular mechanism of PXR binding. For these reasons, we focused in this study on the strong binders versus non-binders of PXR.

In this study, we examined the relationship between the physical/chemical properties of 37 marketed drugs and their interaction with PXR. Among the molecular descriptors, the molecular weight appears to be a useful marker in defining the likelihood of strong binding to PXR. Compounds with molecular weights less than 300 Da appear to be too small to have meaningful interactions with PXR. This is clearly demonstrated by comparing the small molecular size of caffeine with the PXR LBD, and points to the fact that as flexible as PXR may be, there is a lower limit to the contraction that can occur to accommodate small ligands. Secondly, the three-dimensional shapes of the compounds appear to be rather crucial for fitting into the PXR LBD. When the shape of the compound mismatches the binding cavity of PXR beyond its level of maximum flexibility, the compound may be unable to meaningfully interact with PXR.

Modeling analysis of the interaction between strong binders and PXR provides many useful insights to the molecular mechanism of the binding. Many of the strong binders display one of multiple hydrogen-bond donor/acceptor potential. Based on the modeling, the hydrogen-bonding appears to be an essential element for high affinity interactions between a ligand and PXR. This is consistent with previous ligand-based modeling studies that one or more hydrogen-bonding interactions may be crucial for ligand binding. It is possible that the hydrogen bond serves as an anchor and those additional hydrophobic interactions may further enhance the binding between the ligand and the LBD of PXR. As most studies emphasize on the flexibility of the LBD of PXR, this study also suggests that ligands may adapt certain flexible conformations in order to fit into the PXR. Ritonavir serves as a good example of this theory. The predicted conformation of ritonavir inside the PXR indicates that the molecule folds back into a more compact three-dimensional conformation, which is rather distinct from the more extended structure that predicted by molecular dynamics. This type of mutual "induced-fit" mechanism may be rather common for the ligand–PXR interaction and may render molecular modeling more difficult and less predictive.

In summary, a unique structural and binding property of nuclear receptors in the NR family is their large and flexibility ligand-binding cavity. It is well known these nuclear receptors (CAR, PXR, PPAR and VDR) can accommodate a wide range of structurally diverse ligands [28]. Recent elucidations of the PXR crystal structure and the co-crystal structures of PXR with various ligands may provide a structural-based drug design method for reduction of (build-out) the PXR activation liability. The most challenging issue appears to be how to use the binding/functional data to aid in the structural drug design. The current study combines the binding/functional information and structure modeling for providing insights into understanding of the ligand–PXR interactions.

References

[1] Evans WE, Relling MV. Pharmacogenomics: translating functional genomics to rational therapeutics. Science 1999;286:487–91.
[2] Cui X, Thomas A, Gerlach V, White RE, Morrison RA, Cheng K-C. Application and interpretation of hPXR screening data: validation of reporter signal requirements for prediction of clinically relevant CYP3A4 inducers. Biochem Pharmacol 2008;76:680–9.
[3] Kliewer SA, Moore JT, Wade L, Staudinger JL, Watson MA, Jones SA, et al. An orphan nuclear receptor activated by pregnanes defines a novel steroid signaling pathway. Cell 1998;92:73–82.
[4] Wilson TM, Kliewer SA. PXR, CAR and drug metabolism. Nat Rev Drug Discov 2002;4:259–66.
[5] Moore JT, Kliewer SA. Use of the nuclear receptor PXR to predict drug interactions. Toxicology 2000;153:1–10.
[6] Watkins RE, Davis-Searles PR, Lambert MH, Redinbo MR. J Mol Biol 2003;331:815–28.
[7] Darimont BD, Wagner RL, Apriletti JW, Stallcup MR, Kushner PJ, Baxter JD, et al. Structure and specificity of nuclear receptor–coactivator interactions. Development 1998;12:3343–56.
[8] Xu HE, Lambert MH, Montana VG, Plunket KD, Moore LB, Collins JL, et al. Structural determinants of ligand binding selectivity between the peroxisome proliferator-activated receptors. Proc Natl Acad Sci U S A 2001;98:13919–24.
[9] Wang W, Prosise WW, Chen L, Taremi SS, Le HV, Madison V, et al. Construction of a fully active PXR–SRC1 tethered protein with increased stability. Protein Eng Des Sel 2008;21:425–33.
[10] Raucy J, Warfe L, Yueh MF, Allen SW. A cell-based reporter gene assay for determining induction of CYP3A4 in a high-volume system. J Pharmacol Exp Ther 2002;303:412–23.
[11] Cui X, Thomas A, Han Y, Palamanda J, Montgomery D, White RE, et al. Quantitative PCR assay for cytochrome P-450 2B and 3A induction in rat precision-cut liver slices: correlation study with induction in vivo. J Pharmacol Toxicol Methods 2005;52:234–43.
[12] Chen J, Tran C, Xiao L, Palamanda J, Klapmuts T, Kumari P, et al. Co-induction of CYP3A12 and 3A26 in dog liver slice by xenobiotics: species difference between human and dog CYP 3A induction. Drug Metab Lett 2009;3:290–7.
[13] Watkins RE, Wisely GB, Moore LB, Collins JL, Lambert MH, Williams SP, et al. The human nuclear xenobiotic receptor PXR: structural determinants of directed promiscuity. Science 2001;292:2329–33.
[14] Watkins RE, Maglich JM, Moore LB, Wisely GB, Noble SM, Davis-Searles PR, et al. 2.1 Å crystal structure of human PXR in complex with the St. John's wort compound hyperforin. Biochemistry 2003;42:1430–8.
[15] Watkins RE, Noble SM, Redinbo MR. Structural insights into the promiscuity and function of the human pregnane X receptor. Curr Opin Drug Discov Dev 2002;5:150–8.
[16] Ekins S, Kholodovych V, Ai N, Sinz M, Gal J, Gera L, et al. Computational discovery of novel low micromolar human pregnane X receptor antagonists. Mol Pharmacol 2008;74:662–72.
[17] Jacobs MN. In silico tools to aid risk assessment of endocrine disrupting chemicals. Toxicology 2004;205:43–53.
[18] Ung CY, Li H, Yap CW, Chen YZ. In silico prediction of pregnane X receptor activators by machine learning approaches. Mol Pharmacol 2007;71:158–68.
[19] Annis DA, Athanasopoulos J, Curran PJ, Felsch JS, Kalghatgi K, Lee WH. An affinity selection-mass spectrometry method for the identification of small molecule ligands from self-encoded combinatorial libraries. Discovery of a novel antagonist of *E. coli* dihydrofolate reductase. Int J Mass Spectrom 2004;238:77–83.
[20] Annis A, Chuang CC, Nazef N. ALIS: an affinity selection-mass spectrometry system for the discovery and characterization of protein–ligand interactions. Methods and Principles in Medicinal Chemistry Mass Spectrometry in Medicinal Chemistry 2007;36:121–56.
[21] Annis DA, Nazef N, Chuang CC, Scott MP, Nash HM. A general technique to rank protein–ligand binding affinities and determine allosteric vs. direct binding site competition in compound mixtures. J Am Chem Soc 2004;126:15495–503.
[22] Annis DA, Shipps GW, Deng Y, Popvici-Muller J, Siddiqui MA, Curran PJ, et al. Method for quantitative protein–ligand affinity measurements in compound mixtures. Anal Chem 2007;79:4538–42.
[23] Buczek O, Krowarsch D, Otlewski J. Thermodynamics of single peptide bond cleavage in bovine pancreatic trypsin inhibitor (BPTI). Protein Sci 2002;11:924–32.
[24] Kliewer SA, Goodwin B, Wilson TM. The nuclear pregnane X receptor: a key regulator of xenobiotic metabolism. Endocr Rev 2002;5:687–702.
[25] Evans RM. The nuclear receptor superfamily: a rosetta stone for physiology. Mol Endocrinol 2005;196:1429–38.
[26] Nolte RT, Wisely GB, Westin S, Cobb JE, Lambert MH, Kurokawa R, et al. Ligand binding and co-activator assembly of the peroxisome proliferator-activated receptor-gamma. Nature 1998;395:137–43.
[27] Gampe RT, Montana VG, Lambert MH, Miller AB, Bledsoe RK, Milburn MV, et al. Asymmetry in the PPARgamma/RXRalpha crystal structure reveals the molecular basis of heterodimerization among nuclear receptors. Mol Cell 2000;5:545–55.
[28] Xiao L, Cui X, Madison V, White RE, Cheng K-C. Insights from a three-dimensional model into ligand binding to constitutive active receptor. Drug Metab Disp 2002;30:951–6.